Improved Hybrid Model for Structural Vibration Control Using MOGA, LSTM, and Digital Twin Technology

Chenhao Liu*
School of Civil Engineering, Henan College of Industry & Information Technology, Jiaozuo 454000, China
E-mail: liuchenhao19952017@163.com
*Corresponding author

Keywords: Building structural vibration, long short-term memory, multi-strategy improved sparrow search algorithm, digital twin technology, genetic algorithm

Received: June 30, 2025

With the acceleration of urbanization, the vibration control of high-rise buildings is becoming increasingly prominent. To address the limitations of traditional methods on convergence and robustness against noise, this study proposes a hybrid intelligent control model that integrates a genetic algorithm with a long short-term memory neural network, while incorporating an improved sparrow search algorithm for parameter refinement and a digital twin framework for bidirectional data-driven control. Numerical experiments using seismic records from the PEER Ground Motion Database demonstrated that the proposed model achieved approximately 20% faster convergence compared with particle swarm optimization, whale optimization, and artificial fish swarm algorithms. The root mean square error of vibration prediction was reduced to 0.0180, the identified stiffness error of each floor remained below 1%, and the total control energy was reduced by about 15%. These results confirm the advantages of the proposed method on prediction accuracy, control efficiency, and stability, and highlight its potential applications in seismic design of high-rise structures and smart construction practices.

Povzetek: Opisan je hibridni inteligentni model za aktivno dušenje vibracij visokih stavb, ki združuje MOGA, LSTM, izboljšani algoritem iskanja z vrabci in digitalni dvojček. Rezultati kažejo bistveno boljšo natančnost napovedi, hitrejšo konvergenco in manjšo porabo kontrolne energije.

1 Introduction

Structural vibration control technology, as a cutting-edge field of science and technology, encompasses multiple disciplines, including civil disaster prevention, automatic control, and materials electronics [1]. Although traditional vibration control technology has solved theoretical complex system control problems, many difficulties still exist in practical engineering fields, such as significant differences between structural control system modeling and actual construction, and low sensor reliability in control algorithms [2]. Currently, with the development of science and technology, building structural vibration control technology has greatly improved, contributing to enhanced seismic resistance and comfort of structures. By adjusting structural vibration control strategies, engineers can find specific solutions to meet project requirements [3]. Structural vibration control strategies not only improve the dynamic performance of structures but also optimize parameter settings [4]. Existing methods include using Euler-Bernoulli beams for system dynamic analysis, building structural models based on the Newton-Euler method, and approximating system dynamics using the assumed mode method for wireless characteristics. These methods have greatly facilitated the design of subsequent controllers [5]. However, they also bring many challenges, such as incomplete controller designs and the inability of building walls to connect with vibration systems. Therefore, in response to difficulties in controlling vibrations of high-rise buildings and the unpredictability of sudden faults, this study constructs a hybrid model for intelligent control of building structural vibration, combining Multi-objective Optimization Genetic Algorithm (MOGA) and Long Short-Term Memory (LSTM) artificial neural network. During the model construction, the Multi-strategy Improved Sparrow Search Algorithm (MISSA) and Digital Twin technology are also utilized to predict and analyze the structural stability. It is expected that this model will greatly improve vibration control in high-rise buildings and have broader application prospects in the field of vibration control.

The innovation and contribution of this research lie in constructing a fusion model framework for intelligent control of building structural vibration based on the existing algorithms. For the first time, multi-objective genetic optimization, temporal depth prediction, global search enhancement, and digital twin technology are organically combined to form a closed-loop mechanism of "prediction - optimization - control". This model can not only improve the accuracy of vibration response prediction and real-time control strategy, but also achieve dynamic simulation of structural safety and fault adaptive capability through digital twin, providing a new approach for intelligent control in complex building scenarios.

2 Related work

In recent years, structural vibration control technologies have evolved from traditional passive devices to intelligent algorithm-driven methods. Passive control, as

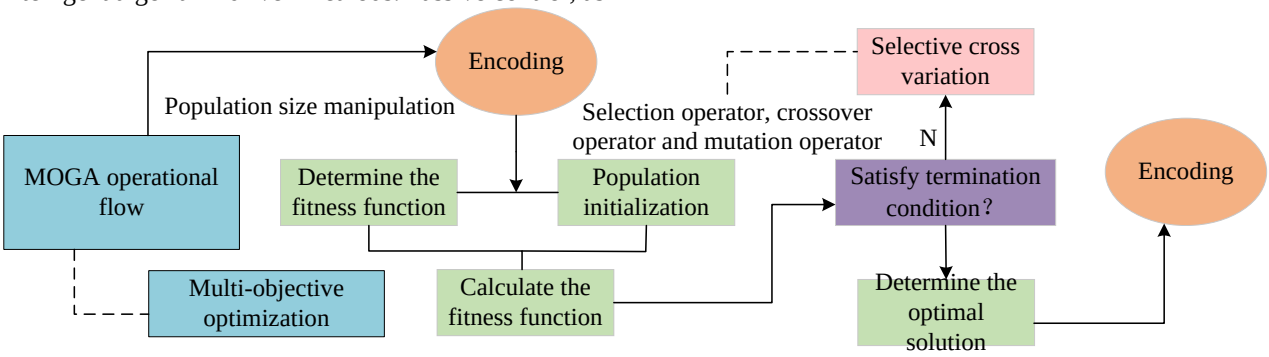

Figure 1: The specific process of the MOGA.

one of the earliest approaches, reduces structural responses by adding damping or mass adjustments. Chowdhury S et al. reviewed inertially amplified passive vibration control devices, demonstrating the potential applications of linear and nonlinear isolation systems in multi-degree-of-freedom structures [6]. Vázquez-Greciano A et al. and Yang F et al. summarized the development of tuned liquid dampers and tuned mass dampers, pointing out their advantages in reducing both horizontal and vertical vibrations, while also highlighting the challenges of optimal design and multi-frequency adaptability [7-8]. In addition, Patsialis D et al. proposed an optimization framework that coupled tuned mass dampers with inerter devices, emphasizing the importance of considering nonlinear behavior in multi-storey structures to improve vibration reduction performance [9].

In the field of semi-active control, magnetorheological dampers have gradually become a research hotspot. Cruze D et al. designed single- and multi-coil dampers and verified their energy dissipation performance under low power consumption, proving their applicability in seismic-resistant buildings and foundation isolation [10]. Bhowmik K et al. combined the LQG control strategy with the Bouc-Wen model to achieve semi-active vibration control of soft-storey buildings, significantly reducing inter-storey responses under various seismic excitations [11]. Kontoni D P N et al. further indicated that tuned mass dampers could effectively mitigate SSI effects in irregular steel high-rise buildings [12]. Zhang C W proposed the Active Rotary Inertia Driver (ARID) system, expanding the application scope of active control in bridges and large structures [13].

With the development of artificial intelligence and data-driven methods, AI-based vibration monitoring and control have gradually emerged. Zar A et al. reviewed the latest advances in vibration-based damage detection methods, pointing out the potential of deep learning in feature extraction and damage identification, while also revealing problems such as overfitting and data insufficiency [14]. AL Houri A et al. focused on the application of artificial intelligence in passive control structure design, emphasizing its advantages in optimizing isolation systems and enhancing disaster resilience [15].

In conclusion, extensive research has been conducted in structural vibration control by scholars worldwide, with notable achievements in vibration control. However, there is limited research on intelligent vibration control for building structures, particularly in areas such as state feature extraction and control goal recognition. Therefore, this study proposes a hybrid model for building structural vibration intelligent control, combining multi-objective optimization and LSTM. The hybrid model performs system parameter identification and control strategy calculation, making structural vibration control more effective and further enhancing the applicability of the control system.

3 Intelligent control of building structural vibration combining MOGA and LSTM

The study considers a multi-storey shear-type high-rise building, where each floor is treated as a single degree-of-freedom, with mass, stiffness, and damping characteristics taken into account. Under external loads such as earthquakes or wind excitations, the structure exhibits inter-storey displacements and accelerations. The control system obtains structural responses through sensors placed on key floors, while actuators apply the control forces. The main objective of this study is to significantly reduce inter story displacement and acceleration under limited maximum control force constraints, thereby ensuring the stability and safety of the structure under extreme load conditions.

3.1 Design of hybrid algorithm based on MOGA and LSTM

The construction industry has now entered the stage of intelligent development, and control algorithms are capable of precisely managing building structures [16]. However, with the continuous increase in the size and complexity of building structures, traditional control

algorithms tend to suffer from overfitting and have difficulty handling complex analyses [17]. To address these issues, this study proposes an intelligent control method that combines MOGA and LSTM, enabling intelligent optimization for complex building structures. The study proposes the following research questions and

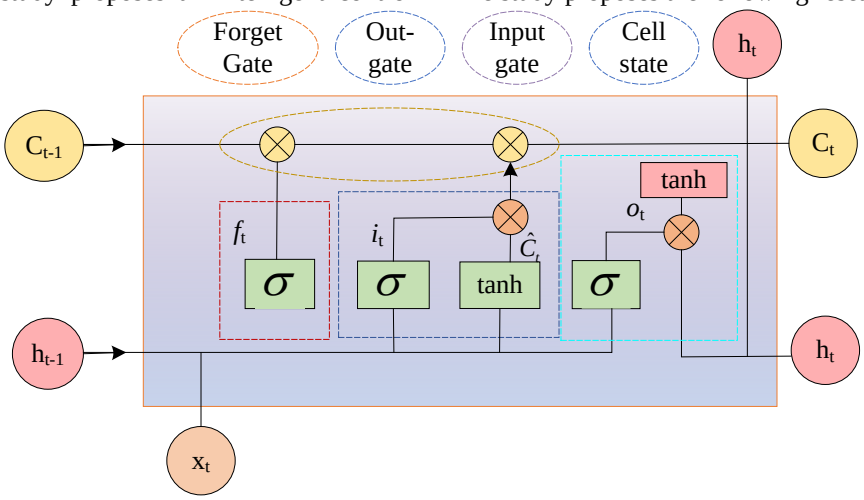

Figure 2: LSTM internal structure.

hypotheses: Can the integration of MOGA and LSTM improve the accuracy and convergence efficiency of structural vibration control? Can MISSA enhance global search ability and avoid local optima? Can digital twin technology improve the generalization and stiffness identification accuracy of the model in complex buildings? Accordingly, three hypotheses are formulated: H1: MOGA-LSTM achieves higher prediction accuracy than some existing optimization algorithms. H2: MISSA improves convergence speed and global optimization performance. H3: Digital twin technology can effectively enhance stiffness identification accuracy.

The specific process of the MOGA is shown in figure 1.

As shown in figure 1, the principle of MOGA is composed of encoding and population initialization, fitness evaluation, selection, crossover, and mutation operations, as shown in figure 1. The crossover and mutation operations in MOGA help with spatial exploration and prevent premature convergence, maintaining population diversity. MOGA can perform single-objective optimization. The fitness function model is denoted in equation (1).

$$\min_{X} J(X) = \alpha PIDR_{\max}(X) + \beta RMS_{acc}(X) + \gamma E_{ctrl}(X) \quad (1)$$

In equation (1), X represents the parameter to be optimized encoded by MOGA. $PIDR_{\max}$ is the peak inter-story displacement ratio, which is used to measure the maximum inter-story deformation of the structure under earthquake action. RMS_{acc} is the root mean square of the floor acceleration, which reflects the comfort and safety of the structural vibration. E_{ctrl} is the control energy, which is obtained by integrating the square of the actuator control force over the entire time history and reflects the control cost. α, β, and γ respectively represent weight coefficients, which are used to balance the importance of the three factors, thereby comprehensively optimizing structural safety, comfort, and economy. The multi-objective optimization setting of MOGA is shown in equation (2).

$$\begin{cases} d_i = \sum_{j=1}^{n} d_i^j \\ I = \{i_1, i_2 \cdots, i_m\} \\ d_{ik}^j = f_j(i_{k+1}) - f_j(i_{k-1}) \end{cases} \quad (2)$$

In equation (2), I represents the individual sequence. i_k denotes the individual. d_i represents the total sum of individual crowding distances. MOGA integrates multiple objective functions, as shown in equation (3).

$$F(x) = \sum_{i=1}^{n} w_i f_i(x) \quad (3)$$

In equation (3), $F(x)$ represents the objective function, and w is the weight vector, with $w_i \geq 0$. MOGA optimizes building load objectives and improves the energy-efficient design of building structures. LSTM captures long-distance data from information and adjusts parameters. Therefore, the study combines the improved GA with LSTM. The internal structure of LSTM is presented in figure 2.

As shown in figure 2, the LSTM mainly consists of the input gate, forget gate, output gate, and cell state. The cell state selectively allows information to pass through or be forgotten, maintaining stability during processing. The forget gate determines which information to discard from the cell state, the input gate updates the cell state, and the output gate decides the output information. Thus, the LSTM can determine the direction of the time series. The updated input gate of LSTM is shown in equation (4).

$$\begin{cases} i_t = \sigma(W_t \times [x_t, h_{t-1}] + b_i) \\ \hat{C}_t = \tanh(W_c \times [x_t, h_{t-1}] + b_i) \end{cases} \quad (4)$$

In equation (4), W_t and W_c represent the weights. b_i and i_t represent the biases, which decide whether the

input gate data can enter the t state. The greatest advantage of LSTM is its memory capability, as it connects both the previous and the subsequent time steps, continuously updating information in the predictive

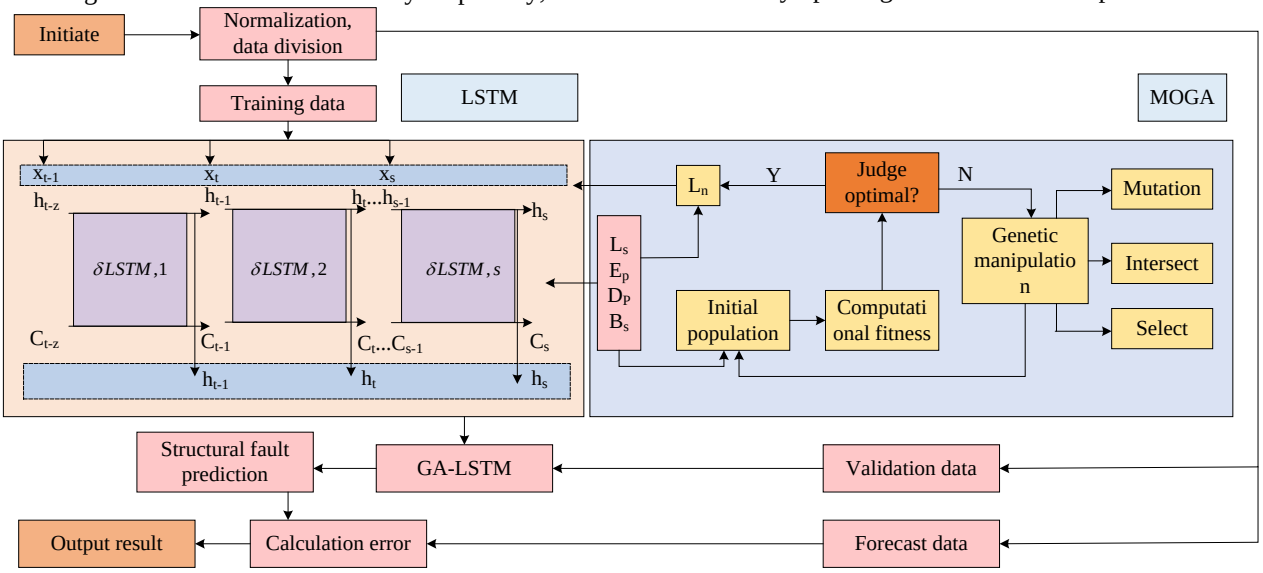

Figure 3: MOGA-LSTM control optimization algorithm flow.

monitoring memory block. Therefore, to address the challenges posed by the complex and variable data of building structures, as well as the potential failures of the building control system, this study combines the global search capability of MOGA and the effective sequence data processing ability of LSTM. This study proposes an MOGA-LSTM-based control optimization algorithm to improve the building structure. The algorithm flowchart is presented in figure 3.

As shown in figure 3, MOGA-LSTM is mainly divided into the input layer, LSTM layer, GA layer, and output layer. First, the data is normalized and divided. Then, the training data is processed, and the hidden data features are extracted through multiple layers of LSTM. Next, the characteristics of MOGA are used to determine the actual parameters of the LSTM layer. Finally, the data from the transmission process is weighted and summed in the output layer, and the error in the structure is calculated. The final output is shown in equation (5).

$$\begin{cases} r_t = \sigma\left(W_r \times \left[x_t, h_{t-1}\right] + b_r\right) \\ h_t = r_t \times \tanh\left(C_t\right) \end{cases} \tag{5}$$

In equation (5), W_r represents the final output weights. b_r represents the final bias of the input gate. h_t represents the final output of the hidden layer. When the forget gate filters the information, the calculation is shown in equation (6).

$$\begin{cases} I_t = \sigma\left(W_I \times \left[x_t, h_{t-1}\right] + b_I\right) \\ C_t = i_t \times \hat{C}_t + I_t \times C_{t-1} \end{cases} \tag{6}$$

In equation (6), at time t, the input to the neuron is x_t. h_t represents the output of the neuron. σ is the activation function of the neuron. I_t is the final result of the forget gate. Therefore, MOGA is primarily employed to perform global optimization of key hyperparameters in LSTM. Its search space covers network structure, learning rate, and batch size, with individuals represented using real-number encoding. The fitness function jointly considers prediction error, inter-story drift suppression, and control energy to achieve multi-objective optimization. Meanwhile, constraints are imposed to ensure that the results satisfy actuator saturation and structural stability requirements, thereby guaranteeing their physical rationality and engineering feasibility.

3.2 Design of hybrid model for building structural vibration intelligent control based on MISSA and digital twin

The vibration stability of building structures plays a decisive role in the quality of buildings. Unavoidable natural disasters pose significant challenges to the design of building structures [19]. Currently, in the field of building structure control, there are issues in control algorithms and actuator development, such as large modeling errors compared to the actual structure and low reliability of control systems [20]. While MOGA-LSTM offers some assistance in optimizing structural data, there are still shortcomings in structural vibration stability. Therefore, to address issues such as the time delay in building structure control forces and prioritization of measurement points, this study improves MOGA-LSTM by incorporating a multi-strategy enhanced sparrow search algorithm for building structural vibration intelligent control. MISSA is mainly embedded as a global optimizer within the MOGA-LSTM model to further refine candidate solutions through local fine-tuning. The optimization parameters mainly focus on the learning rate of LSTM and the distribution of hidden neurons, aiming to improve the convergence speed and stability of the model under complex seismic excitations. MISSA is activated after MOGA converges to a near-optimal solution, and it enhances population diversity through chaotic initialization, sine-cosine updates, and Lévy flight

strategies, thereby avoiding local optima and achieving superior hyperparameter configurations in the

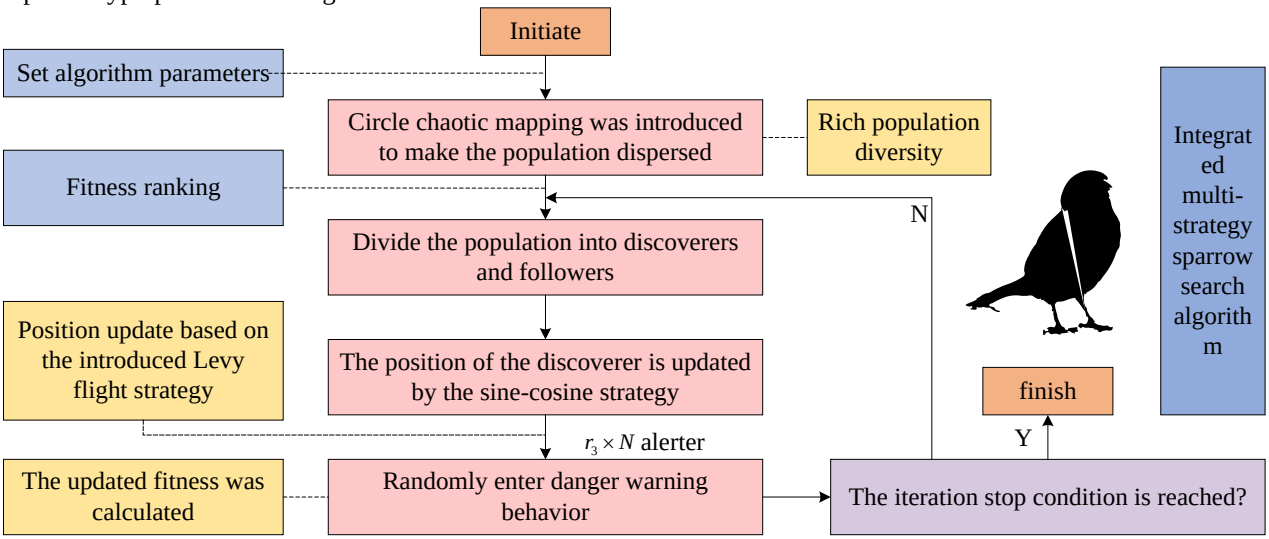

Figure 4: Specific flow of MISSA.

later iterations. The improved Circle chaotic mapping initialization of the population is shown in equation (7).

$$X_{k+1} = \mathrm{mod}\left[d_1 x_k + d_2 - \frac{d_3}{d_1 \pi} \sin\left(d_1 \pi X_k\right), 1 \right] \tag{7}$$

In equation (7), k represents the dimension of the solution. d_1, d_2, and d_3 represent the parameters. The position of the MISSA discoverer is improved by incorporating the cosine-sine algorithm. The update calculation is shown in equation (8).

$$\begin{cases} \omega = \omega_{\min} + \left(\omega_{\max} - \omega_{\min}\right) \cdot \sin\left(t\pi / T_{\max}\right) \\ X_{n,m}^{t+1} = \begin{cases} \left(1-\omega\right) \cdot X_{n,m}^{t} + \omega \cdot \sin\left(r_1\right) \cdot \left| r_2 \cdot X_{best} - X_{n,m}^{t} \right|, R_2 < ST \\ \left(1-\omega\right) \cdot X_{n,m}^{t} + \omega \cdot \cos\left(r_1\right) \cdot \left| r_2 \cdot X_{best} - X_{n,m}^{t} \right|, R_2 \geq ST \end{cases} \end{cases} \tag{8}$$

In equation (8), t represents the number of iterations. ω is the nonlinear decreasing factor, $X_{n,m}^{t}$ is the position of the n-th sparrow at the t-th iteration in the m-th dimension, and r_1 represents the random number on $0 \sim 2\pi$. MISSA adopts the Lévy flight strategy to improve optimization accuracy. The position update for the joiner is shown in equation (9).

$$\begin{cases} Levy\left(x\right) = \dfrac{0.01u}{\left|v\right|^{\frac{1}{\xi}}} \\ x_{n,m}^{t+1} = x_{best}^{t} + \left(x_{best}^{t} - x_{worst}^{t}\right) \cdot \lambda \cdot Levy\left(d\right) \end{cases} \tag{9}$$

In equation (9), ξ ranges within $\left[1,3\right]$. λ is a random number between $0 \sim 1$. d represents the problem dimension to be solved. The position update for the sentinel in MISSA is shown in equation (10).

$$X_{n,m}^{t+1} = \begin{cases} X_{best}^{t} + \beta \cdot \left| X_{n,m}^{t} - X_{best}^{t} \right|, if, f_n > f_g \\ X_{n,m}^{t} + K \cdot \left(\dfrac{\left| X_{n,m}^{t} - X_{worst}^{t} \right|}{\left(f_n - f_w\right) + \varepsilon} \right), if, f_n = f_g \end{cases} \tag{10}$$

In equation (10), X_{best}^{t} represents the best position, β is a normally distributed random number, and 1 is the variance value. f_n represents the fitness value of the n-th individual, where f_g represents the best fitness and f_w represents the worst fitness. In summary, MISSA can perform global optimization on complex structural data and avoid the local optima. The specific process of MISSA is shown in figure 4.

In figure 4, the sparrow algorithm improved with multiple strategies initializes the population by using circle chaotic mapping. After initializing the population, the positions of discoverers and joiners are updated using the cosine strategy and Lévy flight strategy. Once the positions are updated, the fitness of the updated positions is calculated. The algorithm then checks whether the individual positions exceed the boundaries of the search space and whether the iteration count satisfies the conditions. As building structural vibrations have poor adaptability to external environments due to time delays during actual control, this study combines the MISSA global search with digital twin technology to perform safety analysis and prediction on the building structural framework, enhancing the intelligent control of building structures. Digital twin technology enables dynamic collaboration of structures and supports virtual physical interaction configuration modeling to achieve structural security and intelligent control. The safety intelligent framework of the digital twin building structure is shown in equation (11).

$$F_{DT} = \left(S_{\mathrm{Pr}}, S_{vm}, P_{td}, L_{fa}, C_n\right) \tag{11}$$

In equation (11), S_{Pr} and S_{vm} represent the physical structure entity and the virtual structure model. P_{td} and L_{fa} represent the twin data processing layer and the functional application layer. C_n represents the connections between the structural components. The

specific structural safety intelligent control framework of digital twin technology is shown in figure 5.

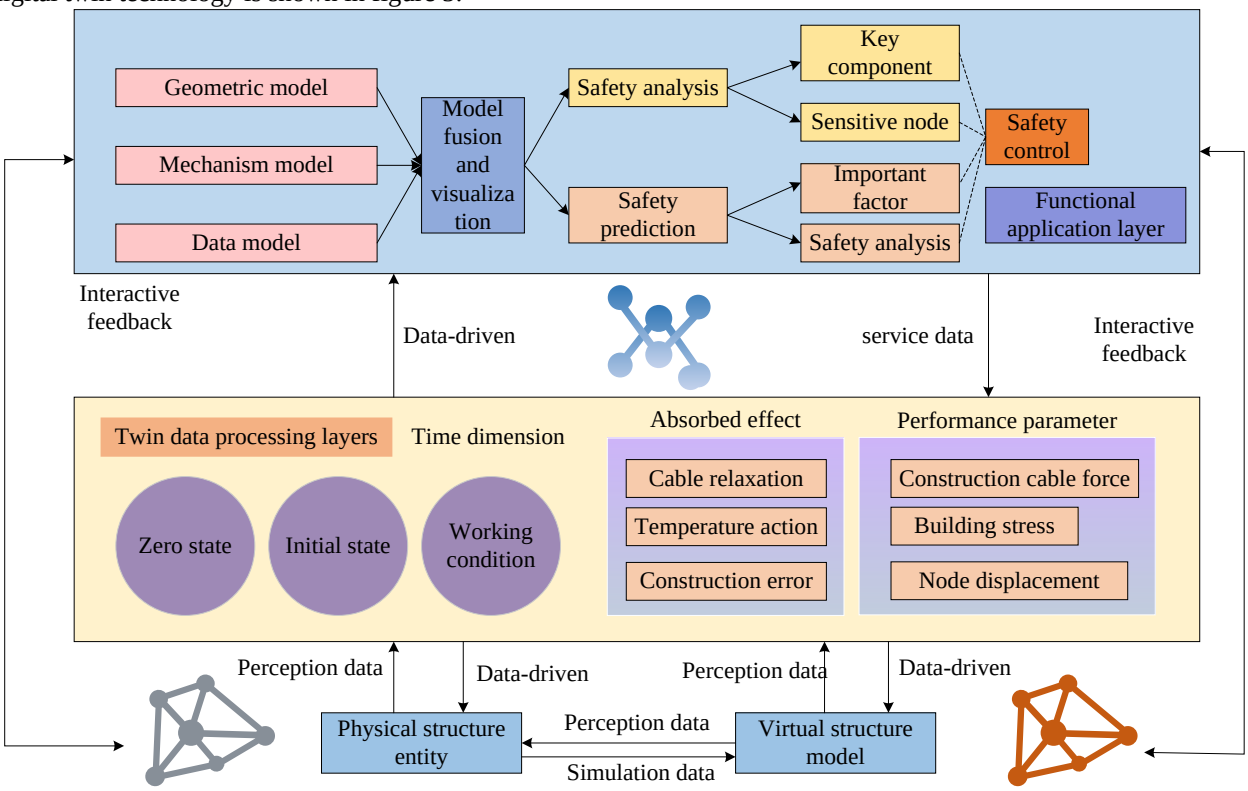

Figure 5: Intelligent control framework for structural safety.

In figure 5, the structure security intelligent framework based on digital twin mainly consists of functional application layer, twin data processing layer, and virtual and physical structure simulation modules. The twin data processing layer incorporates both temporal and spatial dimensions. In the temporal dimension, vibration response data are collected in real-time by sensors and transmitted to the twin, where the virtual model dynamically updates its state based on the physical data and then feeds the corrected prediction back to the physical structure, thereby achieving bidirectional synchronization between the virtual and physical systems. In the spatial dimension, the twin model simultaneously analyzes load-bearing parameters and performance parameters to assess the overall structural safety. With regard to the data processing pipeline, the twin sequentially executes data acquisition, cleaning, feature extraction, prediction, and comparison with subsequent correction. To address sensor noise and model uncertainty, error correction methods and confidence interval constraints are applied, which improves stability and reliability. Furthermore, real-time constraints such as upper limits on sampling frequency and feedback delay have been introduced to ensure that prediction and control commands can be applied to physical structures within acceptable engineering time windows.

The digital twin assumes different roles at different stages. During the training stage, it generates or augments diverse datasets based on the virtual model to enhance the generalization capability of the MOGA-LSTM. During the inference stage, the outputs of the MOGA-LSTM are compared with the simulation results of the virtual model. The global optimization ability of MISSA is employed to refine parameters and update strategies. Through this approach, digital twin can not only intelligently analyze building structures, but also reduce modeling errors in design and construction processes, thereby improving safety prediction and control performance under complex environmental conditions. The specific expression of its safety control is given in equation (12).

$$f(\varphi_1,\varphi_2,\cdots,\varphi_m)\xrightarrow{R}g(\mu_1,\mu_2,\cdots,\mu_m) \tag{12}$$

In equation (12), $f(\varphi_1,\varphi_2,\cdots,\varphi_m)$ represents the set of mechanical parameters. R denotes the limits within the parameter specifications. $g(\mu_1,\mu_2,\cdots,\mu_m)$ represents the set of intelligent control measures. Therefore, to address issues such as the time-varying nature of building material properties and unstable safety performance, this study combines MOGA-LSTM with global optimization and digital twin technology of MISSA for prediction and simulation. A hybrid model based on MISSA and digital twin is developed for intelligent vibration control of building structures. The mechanism of this model integration is shown in figure 6.

From figure 6, digital twin technology enables simulation and measurement output, while the combination of MISSA and MOGA-LSTM allows for safety prediction and key parameter setting of the structure. The data is then analyzed and predicted intelligently, and transmitted to the multidimensional

physical system for precise execution. Driven by digital twin and MISSA algorithms, a hybrid model of

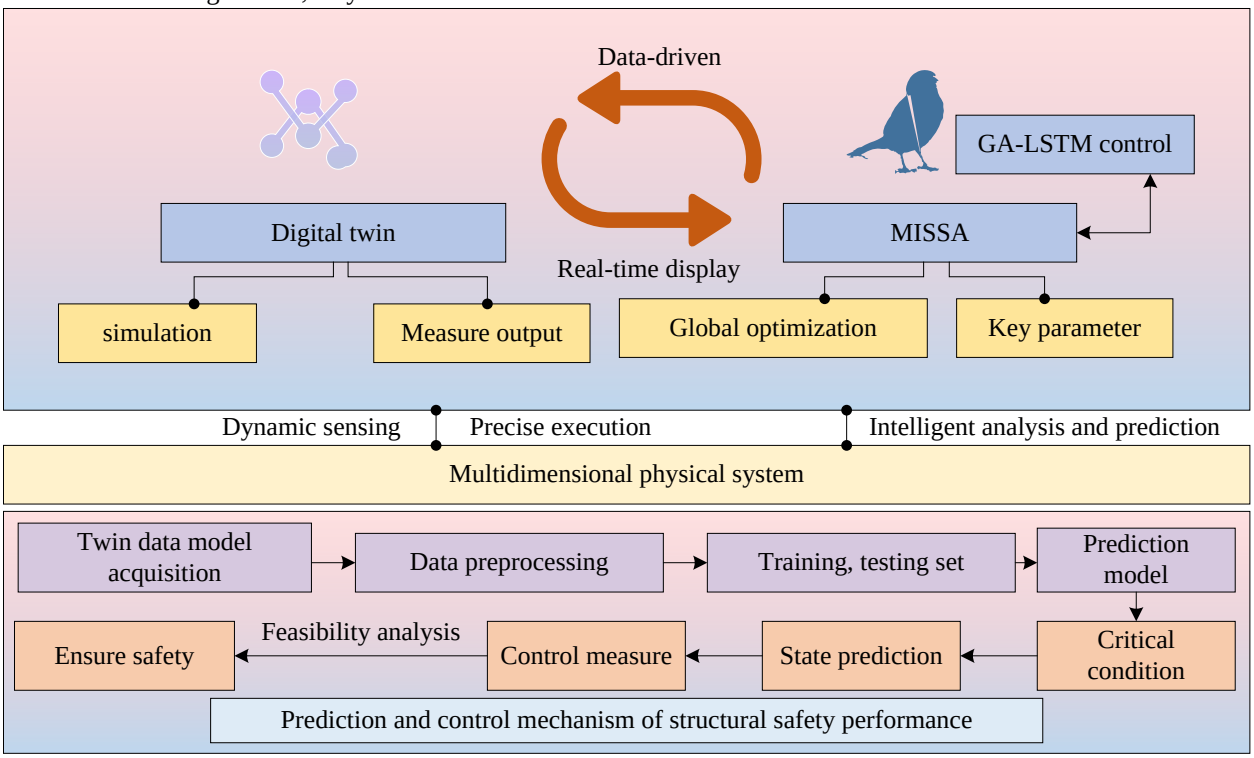

Figure 6: Structure intelligent control hybrid model framework.

intelligent vibration control for building structures based on MISSA and digital twin can detect and capture unsafe factors in the structure, thereby controlling the key factors of building structural vibration.

4 Performance verification of the improved hybrid model for intelligent vibration control of building structures

4.1 Comparison and analysis of MOGA-LSTM performance

To highlight the superior performance of MOGA-LSTM, the study compared it with Particle Swarm Optimization (PSO), Whale Optimization Algorithm (WOA), and Artificial Fish Swarm Algorithm (AFSA). In terms of the experimental environment, Matlab R2019b is used as the primary software, supplemented by Python 3.9. The deep learning framework is PyTorch 1.12.1, with GPU acceleration enabled by CUDA 11.6. Numerical computation and data processing rely on NumPy 1.21 and SciPy 1.7, while visualization is carried out using Matplotlib 3.5 and Seaborn 0.11. The hardware configuration includes an Intel i7-12650H @ 2.30GHz CPU, an NVIDIA RTX 3070 GPU, and 32 GB of memory, running on the Windows 11 operating system. In terms of algorithm parameter settings, to ensure fairness, the maximum number of iterations for all optimization algorithms is set to 100, and the fitness function evaluation criteria are kept consistent. For PSO, the population size is 50, the inertia weight is 0.7, and both learning factors c1 and c2 are set to 1.5. For WOA, the population size is 50, and the encircling parameter decreases linearly. For AFSA, the fish school size is 50, the visual range is 5, the step length is 0.5, and the crowding factor threshold is 0.75. In the MOGA-LSTM, the genetic algorithm takes a population size of 100, a crossover probability of 0.8, and a mutation probability of 0.1. The maximum number of iterations is also set to 100. The LSTM network consists of two hidden layers with 128 neurons each, a learning rate of 0.001, and a batch size of 64. All methods are run with the same data split and random seed to ensure fairness and reproducibility of the experimental results.

The study employs two public datasets, namely the PEER Ground Motion Database and the IASC-ASCE SHM Benchmark Dataset. The former contains typical seismic acceleration time-history records, which are used to verify the model's vibration prediction and control performance under earthquake loads. The latter provides frame structural vibration response data from a structural health monitoring benchmark, which are used to train and test the model's parameter identification and control performance. To validate the convergence performance of the MOGA-LSTM hybrid algorithm in building structures, the four control algorithms, including PSO, WOA, AFSA, and MOGA-LSTM, are tested using the Schaffer benchmark function, and the test results are shown in figure 7.

As shown in figure 7(a), AFSA achieved complete convergence under the Schaffer benchmark function after 40 iterations, while PSO and WOA converged between the 20th and 40th iterations. In contrast, MOGA-LSTM

remained relatively stable throughout the entire 100 iterations. From figure 7(b), it was evident that MOGA-

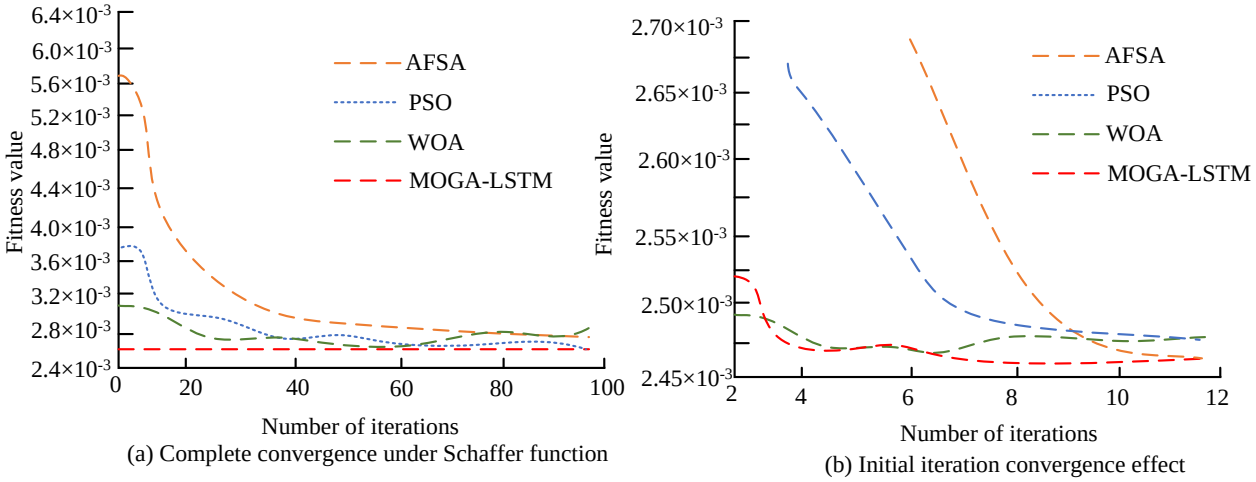

(a) Complete convergence under Schaffer function

(b) Initial iteration convergence effect

Figure 7: Algorithm convergence under Schaffer benchmark function.

Table 1: Results of ablation experiment.

Configuration	Convergence Iterations	Best Validation RMSE	RMSE Std
(i) LSTM only	100 ± 0	0.0320	0.0040
(ii) LSTM + MOGA	95 ± 3	0.0241	0.0021
(iii) LSTM + MISSA	92 ± 4	0.0232	0.0025
(iv) LSTM + MOGA + MISSA	78 ± 5	0.0190	0.0014
(v) LSTM + MOGA + MISSA + Digital twin	68 ± 4	0.0180	0.0012

LSTM converged after 6 iterations, while PSO, WOA, and AFSA all showed less effective convergence. Therefore, MOGA-LSTM demonstrated lower training errors and better convergence performance. Further ablation experiments are conducted, and the results are shown in Table 1.

From Table 1, with the progressive introduction of GA, MISSA, and the digital twin module, the model exhibited clear improvements in convergence speed, prediction accuracy, and stability. When GA or MISSA was added, the number of iterations decreased and the validation error was reduced, indicating that both global search and local refinement enhanced model performance. When GA and MISSA were combined, the convergence was significantly accelerated, errors were further reduced, and the results became more stable. After adding the digital twin, the model achieved the best performance on convergence efficiency and prediction accuracy, while also maintaining high consistency across multiple runs. In summary, the complete framework performed best across all metrics, confirming the necessity and effectiveness of incorporating each module.

To better illustrate the prediction performance of MOGA-LSTM in building structural control, this study takes floor acceleration response as the primary prediction variable. The data is sourced from the PEER Ground Motion Database (such as the El Centro seismic records), which drives the vibration response of the IASC-ASCE benchmark frame structure. All seismic records are sampled at a rate of 0.01 s, with a total duration of 60 s. The data is divided into 70% for training, 15% for validation, and 15% for testing, and zero mean Gaussian noise and 0.005g standard deviation are added to the test set to simulate sensor measurement errors. The predicted values and true values of PSO, WOA, AFSA, and MOGA-LSTM are compared, and the results are shown in Figure 8.

As shown in figure 8(a), the predicted values of AFSA for sample 1 mainly concentrated in the central region, with error fluctuations predominantly in the range of 40-45. In figure 8(b), PSO exhibited larger error fluctuations for sample data between 15 and 50, and the error was more evident when compared to the real values. In figure 8(c), WOA showed significant error fluctuations between sample data 25 and 75, with clear up-and-down variations. However, as shown in figure 8(d), MOGA-LSTM's predicted values aligned closely with the real values, with a prediction accuracy of 97.56%. Therefore, MOGA-LSTM achieved higher prediction accuracy, smaller error fluctuations, and better data control analysis. To further highlight the prediction performance in building structures, the study also compared the mean squared error and prediction error for PSO, WOA, AFSA, and MOGA-LSTM. In addition to these four algorithms, Multiple Objective Particle Swarm Optimization (MOPSO) and Spider Wasp Optimizer (SWO) are added to increase the diversity of the comparison results. The comparison results are shown in Table 2.

As shown in Table 2, PSO had the longest running time at 51s, with the maximum relative error reaching 61.24%. MOGA-LSTM had the shortest running time at 13s, with a root mean square error of 1.248 and a maximum relative error of 15.142%. MOPSO had the

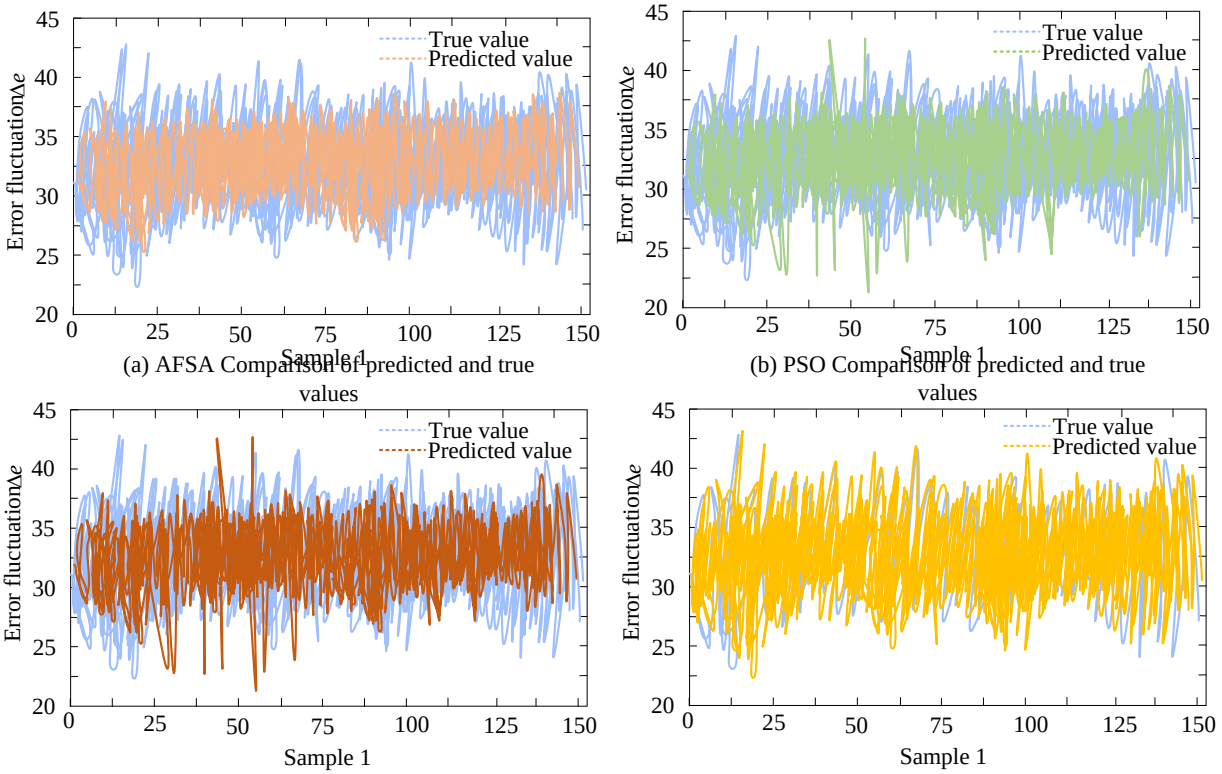

(a) AFSA Comparison of predicted and true values

(b) PSO Comparison of predicted and true values

(c)WOA Comparison of predicted and true values

(d) MOGA-LSTM Mixing Comparison of predicted and true values

Figure 8: Predicted state comparison chart.

Table 2: Comparison of mean square error and prediction error results.

Algorithm	Running time/s	Root mean square error	Maximum relative error/%	Mean absolute error/%	Mean relative error/%
PSO	51	5.014	61.245	5.210	11.487
WOA	43	4.348	48.361	4.168	7.468
AFSA	60	4.126	34.786	4.032	6.875
MOGA-LSTM	13	1.248	15.142	1.478	4.210
MOPSO	25	3.216	26.132	2.676	5.168
SWO	36	2.487	30.456	2.148	5.014

second longest running time at 25s, with a mean relative error of 5.168%. The mean relative error of SWO was very close to MOPSO, with a difference of only 0.514%. The MOGA-LSTM hybrid algorithm demonstrated higher operational efficiency in building structure control, better handling data errors, and strengthening structure failure prediction.

4.2 Performance analysis of the hybrid model for intelligent vibration control of building structures with integrated algorithms

To further verify the superior performance of the building structural vibration intelligent control model based on MOGA-LSTM, it is compared with the building structural vibration intelligent control models constructed using PSO, WOA, and AFSA algorithms. Since the building structural vibration control system is susceptible to natural factors, which can lead to structural safety instability, the study tests the generalization performance of the MOGA-LSTM-based building structural vibration intelligent control model. In the simulation, the control force is generated by active mass dampers installed at the top and critical floors of the structure. To ensure engineering feasibility, the maximum control force is set to 1×108 N, while considering force and velocity saturation constraints. All stiffness parameters are expressed in N/m, and control forces are expressed in N to maintain consistency in physical units. The uncontrolled structural response is selected as the baseline for evaluating the relative improvement achieved by the proposed control strategy. The results for models constructed using MOGA-LSTM, PSO, WOA, and AFSA are shown in figure 9.

From figure 9(a), influenced by the Kobe wave, the control force of the MOGA-LSTM model was close to the original applied force. The WOA model showed a maximum control force of 2×107 N at the 11th floor. From figure 9(b), the AFSA model showed a maximum control force of 3×107 N at the 16th floor, with a significant error compared to the original maximum control force calculation. In conclusion, the MOGA-LSTM model exhibited better generalization

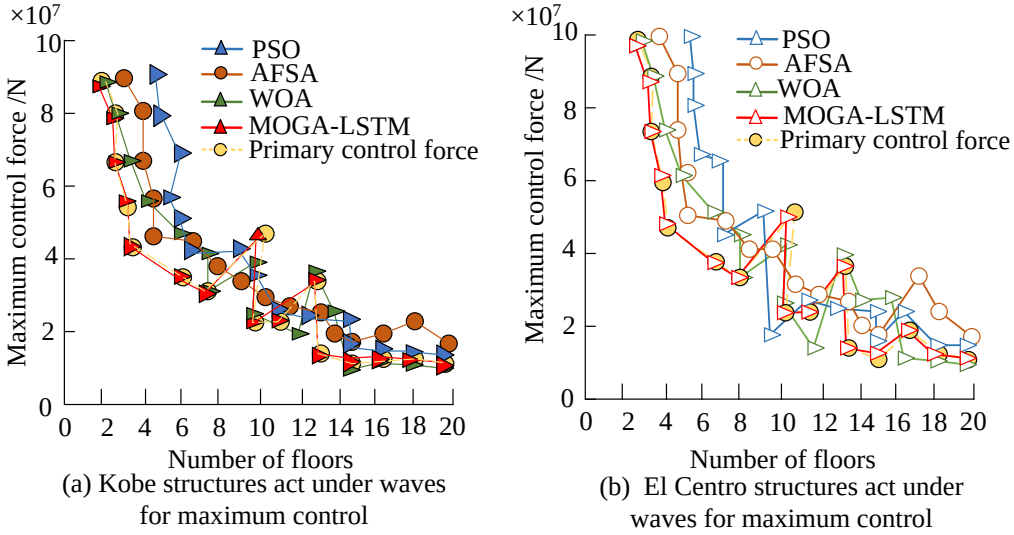

(a) Kobe structures act under waves for maximum control

(b) El Centro structures act under waves for maximum control

Figure 9: Generalized performance test.

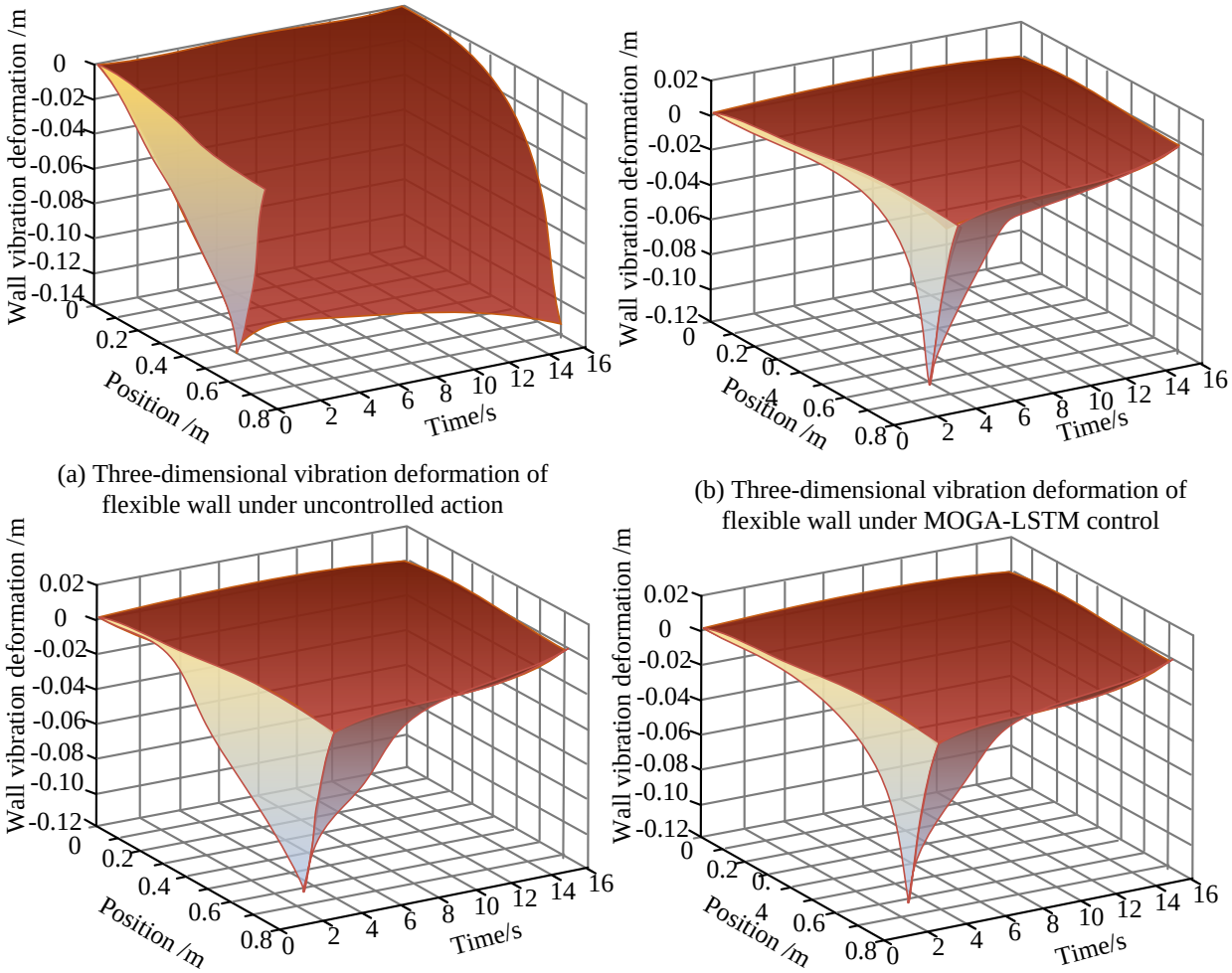

(a) Three-dimensional vibration deformation of flexible wall under uncontrolled action

(b) Three-dimensional vibration deformation of flexible wall under MOGA-LSTM control

(c) Three-dimensional vibration deformation of flexible wall under PSO control

(d) Three-dimensional vibration deformation of flexible wall under WOA control

Figure 10: Comparison of 3D vibration deformation curve of flexible wall.

performance and stronger control adaptability. To further verify the control performance of the MOGA-LSTM model, it is compared with the PSO and WOA models through a three-dimensional simulation experiment of a flexible wall. The simulation results are shown in figure 10.

Table 3: Stiffness identification of each floor.

Floor	1	2	3	4	5	6	7	8	9	10
True stiffness	3.28	8.64	8.64	8.64	7.12	5.68	5.68	5.67	5.67	5.67
Identified stiffness	3.271	8.634	8.650	8.634	7.116	5.674	5.671	5.664	5.664	5.650
Floor	11	12	13	14	15	16	17	18	19	20
True stiffness	5.00	5.00	5.00	3.94	2.97	2.97	2.97	2.97	2.35	1.90
Identified stiffness	4.981	5.041	5.004	3.954	2.961	2.964	2.965	2.981	2.341	1.910

Table 4: Comparison of control performance for different methods on a 20-floor building.

Method	Peak PIDR (%)	RMS Acceleration (m/s2)	Control Energy (N·m)	Stabilization Time (s)
Uncontrolled	2.85	0.412	/	12.4
TMD	2.10	0.326	/	10.6
LQR	1.75	0.298	1.24×106	8.7
MOGA-LSTM	1.42	0.251	9.85×105	5.3

In the 3D simulation of the flexible wall shown in Figure 10, the wall height, width, and thickness were set according to typical frame structure parameters, with the base fixed and the top free. The model was discretized using a finite element mesh, and damping characteristics were represented by a Rayleigh model that considered both material and structural damping. Control forces were subject to saturation and rate limits, sensors were placed at the top and mid-height of the wall to monitor displacement and acceleration, and the Newmark-β method was used to ensure numerical stability. From figure 10(a), under the initial condition, the vibration deformation of the single-floor building without control could not converge to 0. From figure 10(b), the MOGA-LSTM model stabilized the wall vibration at 5 s. Figure 10(c) showed that the PSO model stabilized the wall vibration at 8 s. Figure 10(d) indicated that the WOA-based building structural vibration control model still showed wall deformation between 4 and 6 s. Therefore, the MOGA-LSTM model effectively suppressed the vibration deformation of the flexible wall and exhibited better convergence. To further validate the parameter identification performance of the MOGA-LSTM model, stiffness identification was conducted for a 20-floor building under the El Centro ground motion. The input ground motion was obtained from the PEER Ground Motion Database, with a sampling rate of 0.01 s and a total duration of 60 s. Gaussian noise with zero mean and a standard deviation of 0.005 g was added to the test data to simulate sensor measurement errors. Stiffness identification was performed using a prediction error minimization-based MOGA-LSTM approach, in which the prediction errors of floor acceleration and displacement were used as the loss function to optimize the LSTM hyperparameters and output the estimated stiffness of each floor, while regularization constraints were incorporated to enhance stability. Each reported result represents the average of 20 independent trials, and relative errors are provided. The identification results are summarized in Table 3.

As shown in Table 3, the identified stiffness error of the MOGA-LSTM model was below 1% for all floors. Specifically, the identified stiffness on the 19th floor was 2.341, while the actual value was 2.35, with a relative error of 0.37%. For the 12th floor, the identified value was 5.041, differing from the true value of 5.00 by 0.82%. These results demonstrate that the proposed hybrid model maintains high stability and accuracy under noisy conditions, effectively identifying the stiffness parameters of high-rise building structures and showing good applicability and robustness in structural vibration control.

To further verify the vibration control performance of the MOGA-LSTM model, comparative experiments are conducted on a 20-floor building under the El Centro and Kobe ground motions. The seismic records were obtained from the PEER Ground Motion Database, with a sampling rate of 0.01 s and a total duration of 60 s. During the simulation process, the saturation and rate limits of the actuator were uniformly applied. The comparison involves a Linear Quadratic Regulator (LQR), a Tuned Mass Damper (TMD), and the proposed MOGA-LSTM model, with the uncontrolled case set as the baseline. The evaluation metrics include Peak Inter-floor Drift Ratio (PIDR), Root Mean Square (RMS) floor acceleration, and total control energy. Each result is averaged over 20 independent trials, and relative errors are reported. The results are summarized in Table 4.

As shown in Table 4, the MOGA-LSTM model outperformed traditional methods across all evaluation metrics. Compared with the uncontrolled case, the peak PIDR was reduced by approximately 50% and the RMS floor acceleration by about 39%. Compared with TMD and LQR, MOGA-LSTM demonstrated a much shorter stabilization time, requiring only 5.3 s to reach steady state. These results indicate that the proposed hybrid model not only achieves significantly better vibration mitigation than classical control methods, but also exhibits stronger engineering applicability on energy efficiency and response stability.

5 Conclusion

To address the long calculation time for control signals and high hardware costs in building structures, this study developed an MOGA-LSTM-based hybrid intelligent control model for structural vibration suppression. The model integrated MISSA and digital twin technology to detect and capture structural safety risks. To evaluate the performance of the hybrid control model, it was compared with PSO, WOA, and AFSA from convergence effects and other aspects. Experimental results showed that the MOGA-LSTM model converged after 6 iterations with a

prediction accuracy of 97.56%. In contrast, the prediction accuracy of PSO, WOA, and AFSA was 92.15%, 94.56%, and 95.12%, respectively, all of which were lower than that of MOGA-LSTM. Furthermore, the MOGA-LSTM-based control model achieved the best control effect on flexible wall structures at 5 s, gradually stabilizing thereafter. In comparison, the PSO- and WOA-based models achieved optimal control at 6 s and 8 s, respectively, which were not as effective as the MOGA-LSTM model.

Overall, the proposed MOGA-LSTM model not only demonstrates favorable convergence and stability in experiments, but also provides a scalable intelligent solution for structural vibration control in buildings. From a state-of-the-art perspective, the model can be deeply integrated with digital twin, IoT-based sensor networks, and intelligent monitoring platforms, thereby laying the foundation for dynamic safety assessment and predictive maintenance throughout the building lifecycle. In practical applications, the approach can be extended to seismic design of high-rise buildings, structural monitoring of bridges and tunnels during construction, risk warning in construction processes, and real-time control and feedback in smart construction environments, highlighting its broad application prospects and practical value in the building technology and construction domains. Although this study did not explore the vibration suppression and intelligent adjustment of multi-floor flexible high-rise building systems, further research in this area is recommended in the future.

References

[1] Yu Zhang, Zeyu Wang, Diana Tazeddinova, Farzad Ebrahimi, Mostafa Habibi, and Hamed Safarpour. Enhancing active vibration control performances in a smart rotary sandwich thick nanostructure conveying viscous fluid flow by a PD controller. Waves in Random and Complex Media, 34(3):1835-1858, 2024. https://doi.org/10.1080/17455030.2021.1948627

[2] Hui Zhang, Wei Sun, Haitao Luo, and Rongfei Zhang. Active vibration control of composite laminates with MFC based on PID-LQR hybrid controller. Mechanics of Advanced Materials and Structures, 31(25):6382-6399, 2024. https://doi.org/10.1080/15376494.2023.2229841

[3] Rui He, and Lijun Pan. Seismic responses and vibration control of offshore wind turbines considering hydrodynamic effects based on underwater shaking table tests. Earthquake Engineering & Structural Dynamics, 53(2):545-572, 2024. https://doi.org/10.1002/eqe.4035

[4] Xingyu Zhou, Haoping Wang, and Yang Tian. Robust adaptive flexible prescribed performance tracking and vibration control for rigid–flexible coupled robotic systems with input quantization. Nonlinear Dynamics, 112(3):1951-1969, 2024. https://doi.org/10.1007/s11071-023-09139-6

[5] Yanli Wang, Xianghong Li, and Yongjun Shen. Study on mechanical vibration control of limit cycle oscillations in the van der Pol oscillator by means of nonlinear energy sink. Journal of Vibration Engineering & Technologies, 12(1):811-819, 2024. https://doi.org/10.1007/s42417-023-00877-w

[6] Sudip Chowdhury, Arnab Banerjee, and Sondipon Adhikari. A critical review on inertially-amplified passive vibration control devices. Archives of Computational Methods in Engineering, 31(4):2139-2175, 2024. https://doi.org/10.1007/s11831-023-10040-z

[7] Andrea Vázquez-Greciano, Antonio Aznar López, Nicola Buratti, and Jesús María Ortiz Herrera. Magnetic fields to enhance tuned liquid damper performance for vibration control: A review. Archives of Computational Methods in Engineering, 31(1):25-45, 2024. https://doi.org/10.1007/s11831-023-09971-4

[8] Fan Yang, Ramin Sedaghati, and Ebrahim Esmailzadeh. Vibration suppression of structures using tuned mass damper technology: A state-of-the-art review. Journal of Vibration and Control, 28(7-8):812-836, 2022. https://doi.org/10.1177/1077546320984305

[9] D Patsialis, A A Taflanidis, and A Giaralis. Tuned-mass-damper-inerter optimal design and performance assessment for multi-storey hysteretic buildings under seismic excitation. Bulletin of Earthquake Engineering, 21(3):1541-1576, 2023. https://doi.org/10.1007/s10518-021-01236-4

[10] Daniel Cruze, Nedunchezhian Krishnaraju, and Balaji Ramalingam. Development of single and multi-coil MR damper subjected to cyclic loading for structural vibration control. Advances in Civil and Architectural Engineering, 15(29):106-119, 2024. https://doi.org/10.13167/2024.30.7

[11] Kamalesh Bhowmik, and Nirmalendu Debnath. Semi-active vibration control of soft-storey building with magnetorheological damper under seismic excitation. Journal of Vibration Engineering & Technologies, 12(4):6943-6961, 2024. https://doi.org/10.1007/s42417-024-01292-5

[12] Denise-Penelope N. Kontoni, and Ahmed Abdelraheem Farghaly. Seismic control of T-shape in plan steel high-rise buildings with SSI effect using tuned mass dampers. Asian Journal of Civil Engineering, 25(2):1725-1739, 2024. https://doi.org/10.1007/s42107-023-00873-1

[13] Chunwei Zhang. The active rotary inertia driver system for flutter vibration control of bridges and various promising applications. Science China Technological Sciences, 66(2):390-405, 2023. https://doi.org/10.1007/s11431-022-2228-0

[14] Ali Zar, Zahoor Hussain, Muhammad Akbar, Timon Rabczuk, Zhibin Lin, Shuang Li, and Bilal Ahmed. Towards vibration-based damage detection of civil engineering structures: overview, challenges, and future prospects. International Journal of Mechanics and Materials in Design, 20(3):591-662, 2024. https://doi.org/10.1007/s10999-023-09692-3

[15] Ausamah al Houri, Ahed Habib, Zaid A. and Al-Sadoon. Artificial intelligence-based design and

analysis of passive control structures: an overview. Journal of Soft Computing in Civil Engineering, 9(3):137-168, 2025. https://doi.org/10.22115/scce.2024.450722.1832

[16] Y X Hao, J Cao, and W Zhang. Active vibration control and optimal position of MFC actuator for the bistable laminates with four points simply support. Archive of Applied Mechanics, 94(12):3825-3847, 2024. https://doi.org/10.1007/s00419-024-02697-0

[17] Binglin Li. Unbalanced vibration control of active magnetic bearing using an active disturbance rejection notch decoupling technique. Journal of Vibration and Control, 30(5):1103-1116, 2024. https://doi.org/10.1177/10775463231156465

[18] Shihua Zhou, Bowen Hou, Lisheng Zheng, Pingzhen Xu, Tianzhuang Yu, and Zhaohui Ren. Nonlinear property and dynamic stability analysis of a novel bio-inspired vibration isolation–absorption structure. Nonlinear Dynamics, 112(2):887-902, 2024. https://doi.org/10.1007/s11071-023-09084-4

[19] Tanmoy Konar. Design of intermediate-depth tuned liquid damper with horizontal baffles for seismic control and carbon footprint reduction of buildings. Journal of Vibration Engineering & Technologies, 12(2):2641-2658, 2024. https://doi.org/10.1007/s42417-023-01005-4

[20] Hongxiang Hu, Lincong Chen, and Jiamin Qian. Random vibration analysis of nonlinear structure with viscoelastic nonlinear energy sink. Journal of Vibration and Control, 30(11):2605-2618, 2024. https://doi.org/10.1177/10775463231181645